Analysis of a Candidate Control Algorithm for a Ride-Quality Augmentation System

Reiner Suikat,* Kent Donaldson,† and David R. Downing‡
University of Kansas, Lawrence, Kansas

This paper presents a detailed anaylsis of a candidate algorithm for a ride-quality augmentation system. The algorithm consists of a full-state feedback control law based on optimal control output weighting, estimators for angle of attack and sideslip, and a maneuvering algorithm. The control law is shown to perform well by both frequency and time domain analysis. The rms vertical acceleration is reduced by about 40% over the whole mission flight envelope. The estimators for the angle of attack and sideslip avoid the often inaccurate or costly direct measurement of those angles. The maneuvering algorithm will allow the augmented airplane to respond to pilot inputs. The design characteristics and performance are documented by the closed-loop eigenvalues; rms levels of vertical, lateral, and longitudinal acceleration; and representative time histories and frequency response.

Nomenclature

$\boldsymbol{A}$ = system dynamics matrix
a = acceleration, ft/s^2
$\boldsymbol{B}$ = control effectiveness matrix
$\boldsymbol{C},\boldsymbol{D}$ = output matrices
C_L = lift coefficient
C_Y = side force coefficient
f = force, lb
g = gravitational acceleration, ft/s^2
h = altitude, ft
J = cost function index
$\boldsymbol{K}$ = gain matrix
L = scale length, ft
$\boldsymbol{M}$ = cross-weighting matrix
m = mass, slugs
p,q,r = angular rates, rad/s
$\boldsymbol{Q}$ = state weighting matrix
$\boldsymbol{R}$ = control weighting matrix
$\boldsymbol{r}$ = disturbance vector
S = reference wing area, ft^2
T = sample time, s
t = time, s
U = total velocity, ft/s
u,v,w = velocity components, ft/s
$\boldsymbol{u}$ = control vector
W = weight, lb
$\boldsymbol{x}$ = state vector
$\boldsymbol{y}$ = output vector
α = angle of attack, rad
β = angle of sideslip, rad
Γ = control effectiveness matrix
$\delta_{df},\delta_r,\delta_a$ = differential flap, rudder, aileron deflection, rad
$\delta_f,\delta_e,\delta_{se}$ = flap, elevator, separate surface elevators deflection, rad
θ = pitch angle, rad
σ = gust intensity, ft/s
Φ = state transition matrix
ϕ = bank angle, rad
Φ_g = power spectral density
ω = frequency, rad/s
$()'$ = transpose
$\bar{()}$ = lateral-directional matrix
$()_{ij}$ = matrix element
$(\hat{})$ = output weighting matrix; estimated quantity

Subscripts

l = trim state
b = body axes
CL = closed loop
g = gust
k = index
m = command model
p = pilot
se = separate surface elevator
x,y,z = coordinate axes
v = lateral
w = vertical

Presented as Paper 87-2936 at the AIAA/AHS/ASEE Aircraft Design, Systems, and Operations Meeting, St. Louis, MO, Sept. 16-18, 1987; received Oct. 27, 1987; revision received May 4, 1988.

*Project Manager, Department of Aerospace Engineering. AIAA Student Member.
†Graduate Research Assistant, Department of Aerospace Engineering. AIAA Student Member.
‡Professor, Department of Aerospace Engineering. Associate Fellow AIAA.

Introduction

FROM 1975 to 1986 the number of passengers carried annually by commuter airplanes in the United States has risen an average of over 17% per year. The increase from 4.64 to 26.72 million passengers[1] has made this segment of the airline industry more important. To attract passengers, the commuters must provide a ride comparable to that of large airliners. The perception of ride quality is basically a function of the vertical and lateral accelerations experienced by the passenger. These accelerations are mainly caused by flying through turbulence. A comfort rating can be defined as[2]:

$$C = 2.1 + 17.2\,\bar{a}_z + 17.1\,\bar{a}_y \tag{1}$$

where $\bar{a}_z$ = rms vertical acceleration and $\bar{a}_y$ = rms lateral acceleration. This comfort rating corresponds to passenger satisfaction as determined by actual passenger surveys. A comfort rating of 4, for example, means that 80% of the passengers will be satisfied with the ride; a rating of 7 corresponds to only 25% passenger satisfaction.

Figure 1 shows the comfort rating of a Cessna 402B open loop over a typical mission flight envelope. It is obvious that for moderate turbulence (probability of exceedance $= 10^{-3}$), only a small percentage of passengers will be satisfied with the ride.

The main factors contributing to an airplane's sensitivity to gusts are its wing loading W/S and lift curve slop C_{L_α}:

$$\bar{a}_z \propto C_{L_\alpha} \frac{\rho u_1}{W/S} \sigma_{g_w} \tag{2a}$$

$$\bar{a}_y \propto C_{Y_b} \frac{\rho u_1}{W/S} \sigma_{g_v} \tag{2b}$$

For commuters, W/S is low because of field length requirements, and C_{L_α} is high because of high aspect ratio wings with little sweep. The equations show that sensitivity to gusts at low altitudes, where these airplanes primarily operate, is higher because of the higher density. In addition to that, the gust intensity σ_g is also higher at low altitudes, as shown in Fig. 2. For these reasons, commuter airplanes are more susceptible to gusts than are jet transports.

The use of gust alleviation systems is not new. Research has been done over the last 30 years for military[3–6] and commerical aircraft.[7–10] A research program to develop and test a ride-quality augmentation system (RQAS) is currently being conducted at the University of Kansas.[11–13] The system uses an active control system to counteract airplane motions caused by turbulence. Candidate controllers are designed for use on a Cessna 402B twin-engine aircraft.

This paper presents the detailed analysis of one of the candidate control designs, output weighting. The analysis is given in the form of performance predictions based on linear simulations and frequency domain analysis (power spectral density).

RQAS Description

The research airplane, a Cessna 402B, will be modified to have a separate-surface elevator and independent inboard and outboard plain flaps, as shown in Fig. 3. All flaps will be used to provide lift control, whereas only the outboard flaps will be driven differentially to provide roll control. A separate-surface rudder is not possible because its full control power is needed to meet engine-out requirements; therefore, the RQAS rudder command will drive the entire rudder through an autopilot servo. The pilot has full control over the standard control surfaces, which have more control power than the separate surfaces. This means that safe operation of the airplane is possible, even in the case of a hardover failure. The pilot can only use the rudder, however, by overpowering the rudder servo slip-clutch.

The proposed RQAS, shown in Fig. 4, uses a digital controller implementing a full-state feedback control law, designed using optimal control. Since a pure regulator design would tend to fight the pilot's commands as it tries to alleviate all accelerations, a special maneuvering algorithm has been developed. This algorithm lets the RQAS ignore accelerations caused by pilot input so that the airplane behaves like an unaugmented airplane with regard to pilot commands. Because full-state feedback is used, a complete sensor package is required. This includes measurements of accelerations, aircraft attitude angles and rates, angle of attack, angle of sideslip, and atmospheric data to compute total velocity. To eliminate the need for angle-of-attack and angle-of-sideslip sensing, estimators will be used that infer angle of attack and sideslip from the vertical and lateral accelerometers. A test engineer's station allows complete control of the system for research purposes.

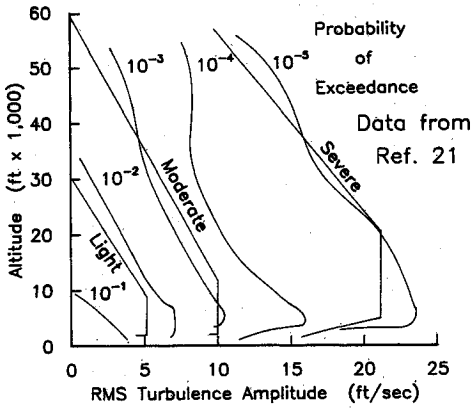

Fig. 2 Variation of gust intensity σ_w with altitude.

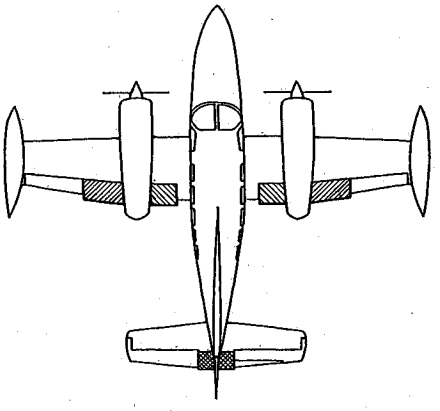

Fig. 3 Research airplane with RQAS control surfaces.

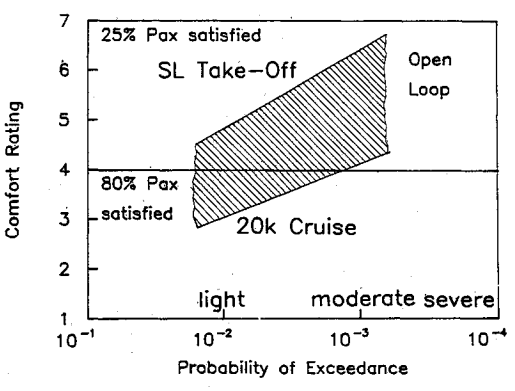

Fig. 1 Comfort rating for open-loop Cessna 402B.

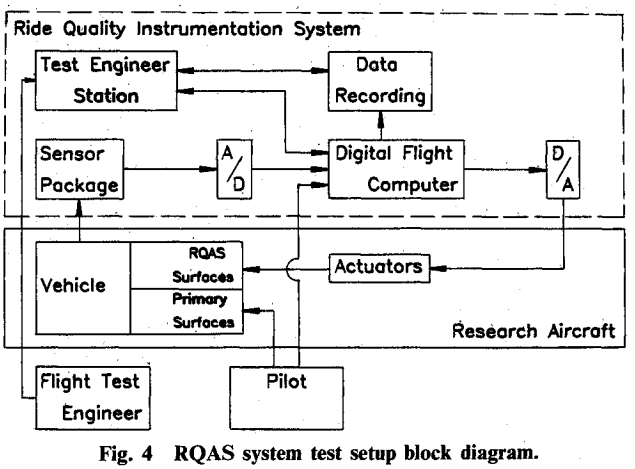

Fig. 4 RQAS system test setup block diagram.

Control Algorithms

Control Law

As stated earlier, the control laws implemented in the system use full-state feedback with gains calculated using optimal control theory. This requires that the airplane be modeled as a set of first-order, linear differential equations in matrix form:

$$\dot{\boldsymbol{x}} = \boldsymbol{A}\boldsymbol{x} + \boldsymbol{B}\boldsymbol{u} \tag{3}$$

where

$$\boldsymbol{x}'_{\text{long}} = [\alpha\, u\, q\, \theta], \qquad \boldsymbol{u}'_{\text{long}} = [\delta_{se}\, \delta_f]$$

$$\boldsymbol{x}'_{\text{lat}} = [\beta\, p\, r\, \phi], \qquad \boldsymbol{u}'_{\text{lat}} = [\delta_{df}\, \delta_r]$$

Note that the longitudinal and lateral-directional equations have been separated. This is a good approximation for most airplanes in straight and level flight. The coefficients of the system dynamics matrix $\boldsymbol{A}$ and the control effectiveness matrix $\boldsymbol{B}$ are found as linearizations of a nonlinear model of the C402B existing at NASA Langley Research Center. Models of the airplane were generated at five different flight conditions spanning a typical mission flight envelope, namely,

1)	takeoff	$h = 0$ ft	$V = 109$ kts
2)	climb	$h = 0$ ft	$V = 125$ kts
3)	climb	$h = 5000$ ft	$V = 135$ kts
4)	cruise	$h = 20{,}000$ ft	$V = 212$ kts
5)	approach	$h = 0$ ft	$V = 108$ kts

Since the controller is implemented in a digital computer, the sampled data regulator approach is used. The controls $\boldsymbol{u}$ are held constant over the sample period, and the output weighting problem[14] is now formulated as follows: Find the control sequence $\boldsymbol{u}_k$, $k = 0,1\ldots$ that will minimize the continuous time cost function

$$J = \frac{1}{2}\int_0^\infty (\boldsymbol{y}'\boldsymbol{Q}\boldsymbol{y} + \boldsymbol{u}_k'\boldsymbol{R}\boldsymbol{u}_k)\, \mathrm{d}t \tag{4}$$

where $\boldsymbol{y}$ is a vector of output quantities given by

$$\boldsymbol{y} = \boldsymbol{C}\boldsymbol{x} + \boldsymbol{D}\boldsymbol{u}$$

and

$$\boldsymbol{u} = \boldsymbol{u}_k = \text{const}, \qquad t_k \leqslant t < t_k + T$$

$\boldsymbol{Q}$ and $\boldsymbol{R}$ are weighting matrices that are chosen to be diagonal matrices. The diagonal elements of these matrices reflect the relative importance of the respective outputs or controls by weighting them in the cost function integral. For a solution to exist, $\boldsymbol{Q}$ must be positive semidefinite and $\boldsymbol{R}$ positive definite.

Using the output vector $\boldsymbol{y}$ in the cost function allows the control designer to weight quantities that are given as a linear combination of states and controls. This is especially useful for a ride-quality augmentation system because the variables of primary interest, i.e., the accelerations, can be expressed as linear combinations of states and controls:

$$a_z = U_1\dot{\alpha} - U_1 \cos(\alpha_1)q + g \sin(\theta_1)\theta \tag{5}$$

Note that $\dot{\alpha}$ can be replaced by the first of the state equations [Eq. (3)] and, hence,

$$a_z = [U_1A_{11}\ \ U_1A_{12}\ \ U_1(A_{13} - \cos\alpha_1)\ \ U_1A_{14} + g\sin\theta_1] \begin{bmatrix} \alpha \\ u \\ q \\ \theta \end{bmatrix} + [U_1B_{11}\ \ U_1B_{12}] \begin{bmatrix} \delta_{se} \\ \delta_f \end{bmatrix} \tag{6}$$

Therefore, a_z can be thought of as an element of the output vector

$$\boldsymbol{y} = \boldsymbol{C}\boldsymbol{x} + \boldsymbol{D}\boldsymbol{u} \tag{7}$$

where

$$\boldsymbol{y}' = \{a_z\, \alpha\, u\, q\, \theta\}$$

The digital-control, continuous-cost-function problem given in Eq. (4) can be shown to be equivalent to a discrete problem[14] that has as its system equation

$$\boldsymbol{x}_{k+1} = \boldsymbol{\Phi}\boldsymbol{x}_k + \boldsymbol{\Gamma}\boldsymbol{u}_k \tag{8}$$

where

$$\boldsymbol{y}_k = \boldsymbol{C}\boldsymbol{x}_k + \boldsymbol{D}\boldsymbol{u}_k$$

$$\boldsymbol{\Phi} = e^{\boldsymbol{A}T}, \qquad \boldsymbol{\Gamma} = \left\{\int_0^\infty (e^{\boldsymbol{A}T})\, \mathrm{d}t\right\}\boldsymbol{B}$$

and that selects the following control sequence to minimize the discrete cost function:

$$J = \sum_0^\infty (\boldsymbol{y}_k'\hat{\boldsymbol{Q}}\boldsymbol{y}_k + \boldsymbol{u}_k'\hat{\boldsymbol{R}}\boldsymbol{u}_k + 2\boldsymbol{y}'\hat{\boldsymbol{M}}\boldsymbol{u}_k) \tag{9}$$

where

$$\hat{\boldsymbol{Q}} = \int_0^T (e^{\boldsymbol{A}'t}\boldsymbol{C}'\boldsymbol{Q}\boldsymbol{C}e^{\boldsymbol{A}t})\, \mathrm{d}t$$

$$\hat{\boldsymbol{M}} = \int_0^T \left[e^{\boldsymbol{A}'t}\boldsymbol{C}'\boldsymbol{Q}\boldsymbol{C}\left(\int_0^T e^{\boldsymbol{A}s}\boldsymbol{B}\, \mathrm{d}s\right) + e^{\boldsymbol{A}'t}\boldsymbol{C}'\boldsymbol{Q}\boldsymbol{D}\right] \mathrm{d}t$$

$$\hat{\boldsymbol{R}} = \int_0^T (\boldsymbol{R}^* + \boldsymbol{N}' + \boldsymbol{N} + \boldsymbol{D}'\boldsymbol{Q}\boldsymbol{D} + \boldsymbol{R})\, \mathrm{d}t$$

$$\boldsymbol{R}^* = \left(\int_0^T \boldsymbol{B}'e^{\boldsymbol{A}'s}\, \mathrm{d}s\right)\boldsymbol{C}'\boldsymbol{Q}\boldsymbol{C}\left(\int_0^t e^{\boldsymbol{A}\tau}\boldsymbol{B}\, \mathrm{d}\tau\right)$$

$$\boldsymbol{N} = \boldsymbol{D}'\boldsymbol{Q}\boldsymbol{C}\left(\int_0^t e^{\boldsymbol{A}\tau}\boldsymbol{B}\, \mathrm{d}\tau\right)$$

For the standard regulator case, where $\boldsymbol{y} = \boldsymbol{x}$, the transformation to the digital domain has been derived by Dorato and Louis.[15] The solution to this problem is the feedback control

$$\boldsymbol{u}_k = -\boldsymbol{K}\boldsymbol{x}_k \tag{10}$$

The algorithm described above is called output weighting (OW) because it allows the direct weighting of any desired quantity that can be expressed as a linear function of the states and controls. Computer programs[16,17] exist to compute these gains from the input matrices $\boldsymbol{A},\boldsymbol{B},\boldsymbol{Q},\boldsymbol{R}$ and the sample time T. The performance of any set of gains is judged from simulation results. The weighting matrices are changed by the designer until a satisfactory design is achieved.

As an example, consider the longitudinal design. The system matrices for flight condition 4 are

$$\boldsymbol{A} = \begin{bmatrix} -1.23 & -0.0005 & 0.958 & 0.0 \\ 18.34 & -0.018 & 0.0 & -32.17 \\ -11.71 & 0.0008 & -7.20 & 0.0 \\ 0.0 & 0.0 & 1.0 & 0.0 \end{bmatrix}$$

$$\boldsymbol{B} = \begin{bmatrix} -0.034 & -0.242 \\ 0.0 & -9.28 \\ -6.97 & 1.55 \\ 0.0 & 0.0 \end{bmatrix}$$

The output vector includes a_z, u, α, q, and θ and is given by

$$y = Cx + Du$$

where

$$C = \begin{bmatrix} -442 & -0.174 & -14.5 & 1.55 \\ 1.0 & 0.0 & 0.0 & 0.0 \\ 0.0 & 1.0 & 0.0 & 0.0 \\ 0.0 & 0.0 & 1.0 & 0.0 \\ 0.0 & 0.0 & 0.0 & 1.0 \end{bmatrix}$$

$$D = \begin{bmatrix} -12.3 & -86.7 \\ 0.0 & 0.0 \\ 0.0 & 0.0 \\ 0.0 & 0.0 \\ 0.0 & 0.0 \end{bmatrix}$$

Using the following values as the diagonal elements of the weighting matrices,

$$Q = [0.05 \quad 10.0 \quad 0.0001 \quad 15.0 \quad 20.0]$$

$$R = [9.6 \quad 3.0]$$

the resulting gains are

$$K = \begin{bmatrix} -0.959 & -0.002 & -0.655 & -0.280 \\ 4.71 & 0.002 & 0.287 & 0.427 \end{bmatrix}$$

Obviously, this is a full-state feedback, which requires every state to be fed back to every control.

Estimators

Full-state feedback requires knowledge of angle of attack and sideslip. By using accelerometer data, the other states, controls, and estimates of angle of attack and sideslip can be computed as a linear combination of those variables.

To obtain the gains for the α estimator, consider the lift equation for small perturbations from steady-state flight given in body axes[18]:

$$m(\dot{w} - U_{b1}q) = -mg\theta \sin\theta_1 + f_z \tag{11}$$

Dividing by m and realizing that

$$\dot{w} \simeq U_1\dot{\alpha} \quad \text{and} \quad U_{b1} = U_1 \cos\alpha_1$$

the equation becomes

$$a_z = U_1\dot{\alpha} - U_1 \cos\alpha_1 q + g \sin\theta_1\theta \tag{12}$$

From the linear model, it follows that

$$\dot{\alpha} = A_{11}\alpha + A_{12}u + A_{13}q + A_{14}\theta + B_{11}\delta_{se} + B_{12}\delta_f + B_{13}\delta_e \tag{13}$$

where A_{ij} and B_{ij} are elements of the system dynamics and control effectiveness matrices. Substituting Eq. (13) into Eq. (12) and solving for α yields

$$\hat{\alpha} = \begin{bmatrix} \frac{1}{U_1A_{11}} & -\frac{A_{12}}{A_{11}} & -\frac{A_{13} - \cos\alpha_1}{A_{11}} & -\frac{A_{14} + (1/U_1)g\sin\theta}{A_{11}} \end{bmatrix} \begin{bmatrix} a_z \\ u \\ q \\ \theta \end{bmatrix} + \begin{bmatrix} -\frac{B_{11}}{A_{11}} & -\frac{B_{12}}{A_{11}} & -\frac{B_{13}}{A_{11}} \end{bmatrix} \begin{bmatrix} \delta_{se} \\ \delta_f \\ \delta_e \end{bmatrix} \tag{14a}$$

In a similar manner, a sideslip estimator can be computed:

$$\hat{\beta} = \begin{bmatrix} \frac{1}{U_1\bar{A}_{11}} & -\frac{\bar{A}_{12} - \sin\alpha_1}{\bar{A}_{11}} & -\frac{\bar{A}_{13} + \cos\alpha_1}{\bar{A}_{11}} & 0 \end{bmatrix} \begin{bmatrix} a_y \\ p \\ r \\ \phi \end{bmatrix} + \begin{bmatrix} -\frac{\bar{B}_{11}}{\bar{A}_{11}} & -\frac{\bar{B}_{12}}{\bar{A}_{11}} & -\frac{\bar{B}_{13}}{\bar{A}_{11}} \end{bmatrix} \begin{bmatrix} \delta_r \\ \delta_{df} \\ \delta_a \end{bmatrix} \tag{14b}$$

Maneuvering Algorithm

As mentioned, a pure regulator will try to cancel all accelerations, including those induced by the pilot. Therefore, it will oppose the pilot when he tries to maneuver the airplane. This opposition can be avoided by using the maneuvering algorithm, which tries to follow a command mode, e.g., the unaugmented airplane. The airplane motion is given as

$$x_{k+1} = \Phi x_k + \Gamma u_k + \Gamma_p u_{pk} \tag{15}$$

where u = RQAS controls and u_p = pilot controls.

A command model also can be generated:

$$x_{mk+1} = \Phi_m x_{mk} + \Gamma_p u_{pk} \tag{16}$$

Using

$$u_k = -K(x_k - x_{mk}) \tag{17}$$

as the controller implementation, the regulator will try to drive the difference between the model states and the actual airplane states to zero. By setting $\Phi_m = \Phi$, the augmented airplane will behave essentially like the open-loop airplane and will not, therefore, counteract the pilot's commands. This formulation requires that the model states be computed at each sample interval; it therefore increases the amount of computations.

Trim Map

All of the preceding algorithms work with perturbation quantities. These are generated from the actual measurements by use of a trim map. This trim map contains the trim values

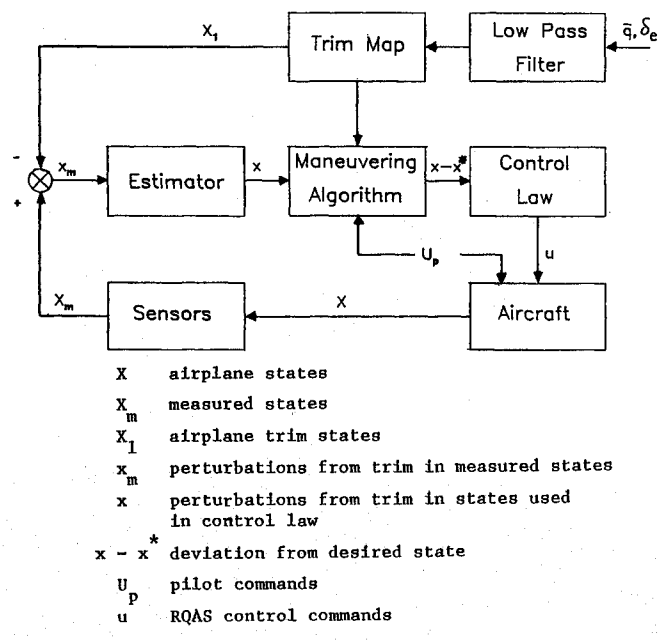

Fig. 5 Simplified algorithm block diagram.

of the longitudinal states for various dynamic pressures $\bar{q}$ and elevator deflections δ_e in two-dimensional data arrays. The lateral states are assumed to have zero trim values. The measurements of $\bar{q}$ and δ_e are passed through a low-pass filter to eliminate the effects of gust and other disturbances, and then the other trim states are computed by a table lookup procedure. The perturbations of all states are simply the differences between the measured states and the trim states. The trim is updated every sample time to avoid transients. A simplified block diagram showing the connections between the various parts of the algorithm is given in Fig. 5.

Projected Performance

The system performance is predicted using a linear time simulation. The linear model is excited by gusts that model a Dryden gust spectrum with a probability of exceedance of 10^{-3}. This corresponds to moderate turbulence. The Dryden spectrum is a commonly used representation of atmospheric turbulence and is given by[19]

$$\Phi_{ag}(\omega) = \sigma_w^2 \frac{L_w}{\pi V_a^3} \frac{1 + 3(L_w\omega/V_a)^2}{[1 + (L_w\omega/V_a)^2]^2} \tag{18}$$

$$\Phi_{\beta g}(\omega) = \sigma_v^2 \frac{L_v}{\pi V_a^3} \frac{1 + 3(L_v\omega/V_a)^2}{[1 + (L_v\omega/V_a)^2]^2} \tag{19}$$

where, for clear-air turbulence, σ_w is taken from Fig. 2 and σ_v is found from the relationship

$$(\sigma_w^2/L_w) = (\sigma_v^2/L_v) \tag{20}$$

where

Above $h = 1750$ ft, $L_w = L_v = 1750$ ft

Below $h = 1750$ ft, $L_w = h$ ft

$L_v = 145(h)^{1/3}$ ft

One way of measuring the performance is to calculate the rms value of the accelerations. This is a simple index that has a direct relation to the passenger comfort rating. It can be seen in Eq. (1) that vertical acceleration $\bar{a}_z$ has almost the same effect on comfort rating as lateral acceleration $\bar{a}_y$. In flight, however, lateral acceleration is usually much smaller because for most airplanes, C_{y_β} is smaller than C_{L_α}, and, as Eq. (1) shows, acceleration caused by gusts is directly proportional to C_{L_α}, and C_{y_β}, respectively. It has been determined from passenger surveys[2] that 80% of airplane passengers will be satisfied if the airplane has a comfort rating of 4. Neglecting lateral acceleration, this corresponds to an rms vertical acceleration of 3.54 ft/s^2, which was chosen as the design goal.

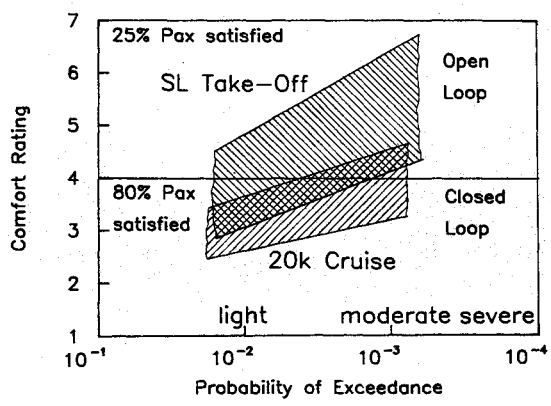

Fig. 6 Comfort rating for open- and closed-loop Cessna 402B.

Figure 6 shows the range of comfort rating for the closed-loop airplane over the mission flight envelope. Because of lateral acceleration, the 80% passenger satisfaction is not achieved over the entire envelope; however, a large increase in passenger satisfaction can be observed.

Figure 7 shows the predicted performance of the RQAS in terms of rms values of a_z, a_x, and a_y. It can be seen that the RQAS achieves a large reduction in both $\bar{a}_z$ and $\bar{a}_y$. The a_z rms reduction is between 40 and 50% for all flight conditions, with the design goal easily met. Note that as the vertical and lateral accelerations are reduced, $\bar{a}_x$ increases. However, its magnitude is quite small.

The main factor limiting the performance is the allowable control activity, more specifically the flap activity. The gains for the cases presented in Fig. 7 have been designed such that certain limits are not exceeded in the simulations. These limits are shown in Table 1. The limits were chosen based on safety considerations required because of the large control power of the flaps, especially in the differential mode, and also to avoid saturation of the control surfaces to reduce the risk of mechanical failures. Because of this, saturation must be avoided in order to reduce the risk of control surfaces having mechanical failures. A gust larger than those used in the design could, however, cause the controller to command the control surfaces beyond these limits. For this reason, the actual controller will include hardware and software limits.

Another way to examine the performance of the system is to look at short samples of a time history. Since the airplane will spend most of its time in cruise, flight condition 4 was chosen to represent typical results. Figure 8 shows the actual values of a_z and a_x open-loop and closed-loop resulting from the Dryden gust field. It is easy to see that on one hand, the RQAS does reduce a_z significantly, while on the other hand, a_x is increased. Since a_x remains very small, this is not of any significance to ride comfort. A closer look shows that the RQAS mainly reduces the low frequency content of the gust, while the high frequencies are not affected. Note that the short peaks, which contain the high-frequency part, are mainly not decreased in magnitude. This is because of the limited bandwidth of the system, which is basically bound by the servo bandwidth. In these simulations, the servos are assumed to have a bandwidth of 10 rad/s.

The flap activity for this case also is plotted in Fig. 8. One can observe that the flaps move at a low frequency that is unable to cancel out the high frequency content of the gust field. The upper limit for the servo bandwidth is mainly dictated by the cost of the actuators. Also, at very high rates of deflection, unsteady aerodynamic effects may cause problems. To determine the effect of very high deflection rates of the control surfaces, their frequency response will be determined with parameter identification flights.

The designs are also evaluated in the frequency domain. Power spectral density plots for a_z, a_x, and a_y caused by gusts are given for flight condition 4 in Fig. 9. It shows that the main contribution to the reduction in $\bar{a}_z$ is in the frequency range that causes motion sickness. For higher frequencies, the curves approach each other. The a_x PSD plot demonstrates the increase in a_x due to the controller. However, the closed-loop $\bar{a}_x$ is still small enough to be of no concern. The α_y PSD plot shows that the controller increases lateral acceleration at

Table 1 Control surface deflection limits

	Maximum deflection/Maximum rate	
	deg	deg/s
Flap	±15	±120
Differential flap	±15	±120
Separate elevator	±5	±50
Rudder	±5	±20

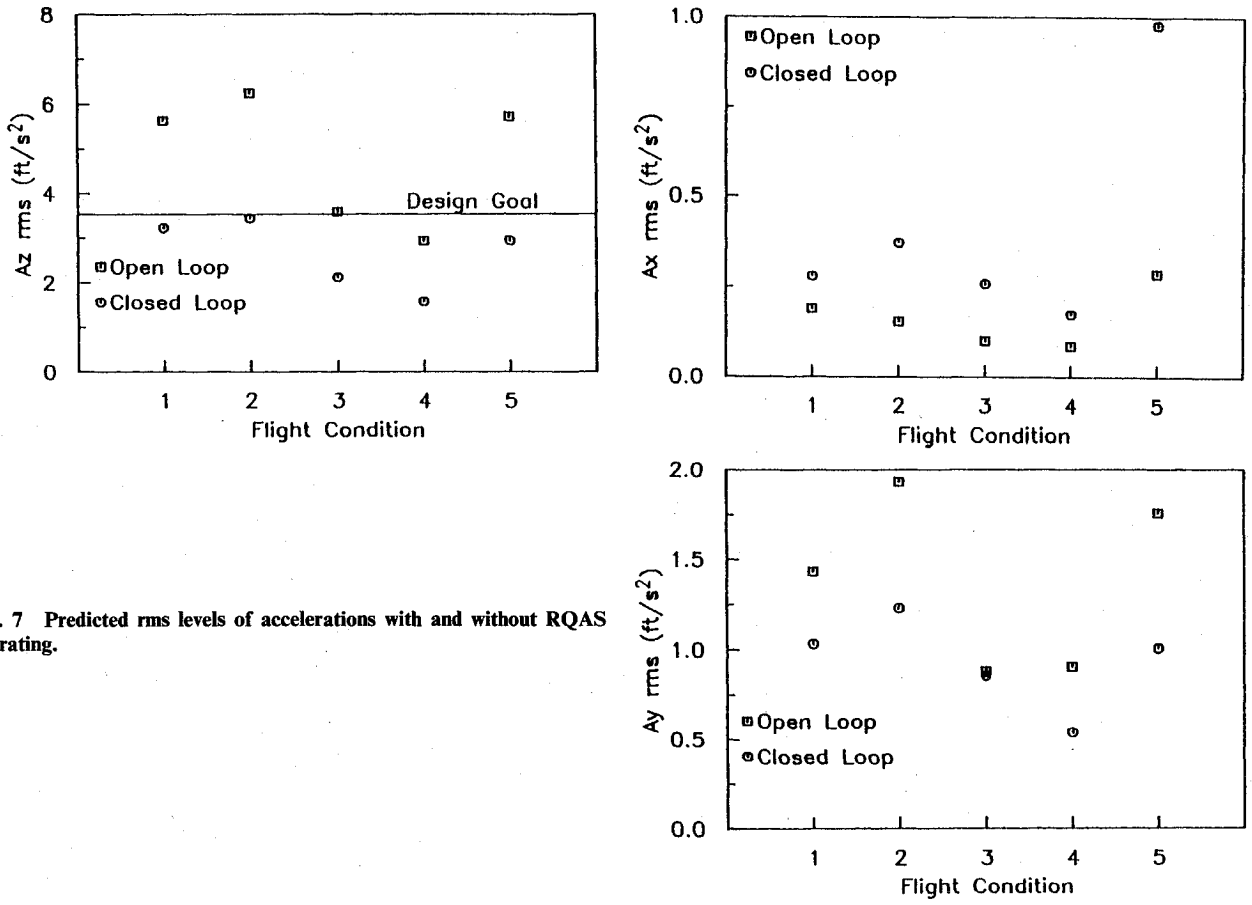

Fig. 7 Predicted rms levels of accelerations with and without RQAS operating.

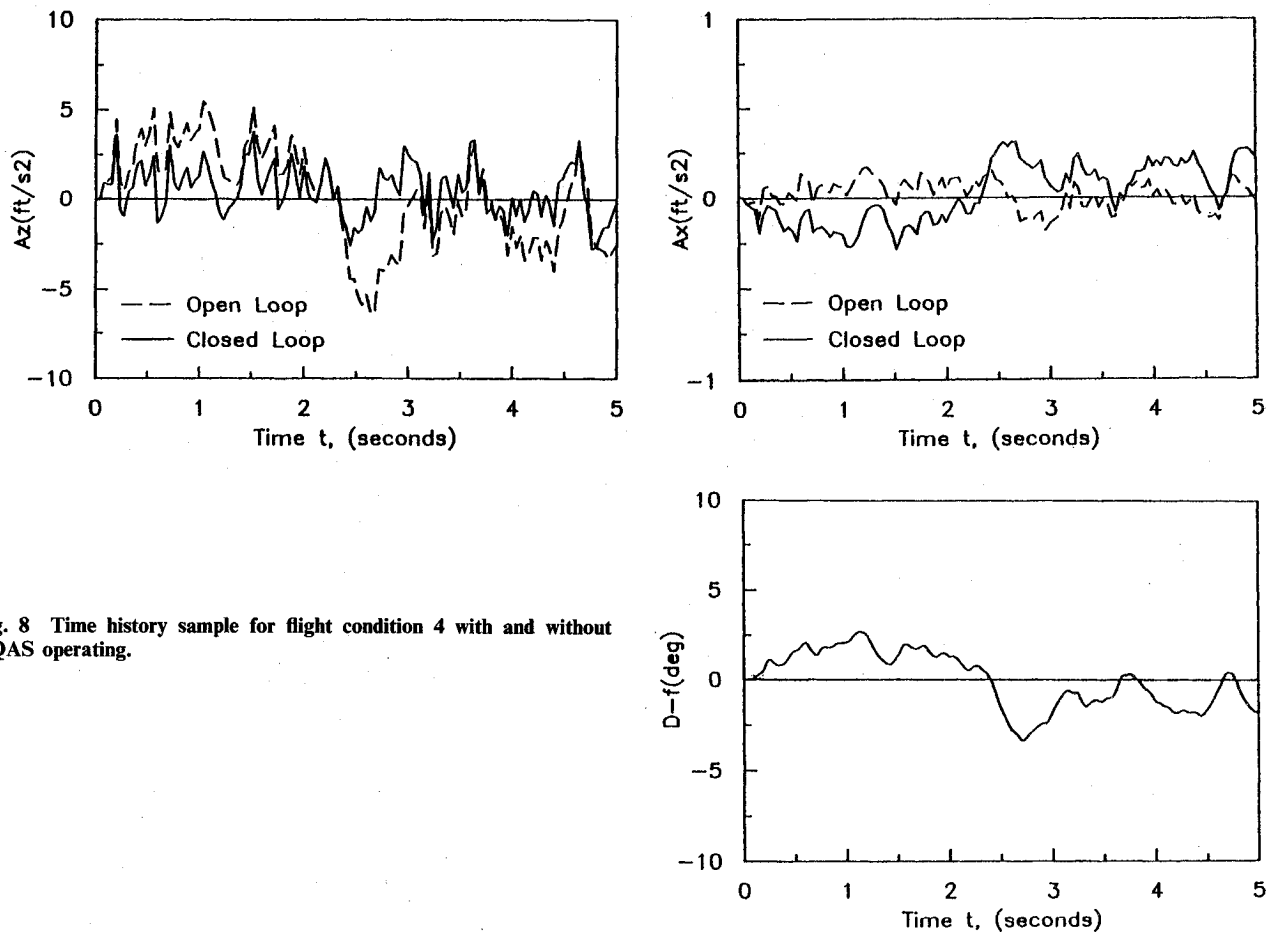

Fig. 8 Time history sample for flight condition 4 with and without RQAS operating.

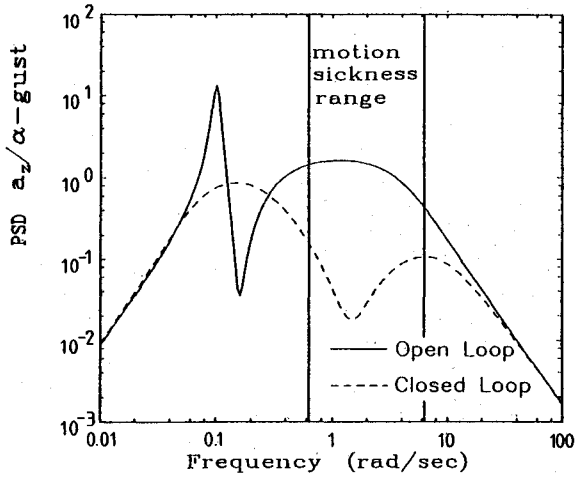

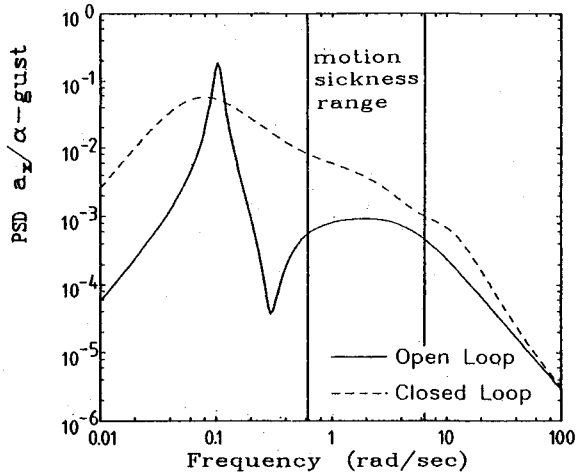

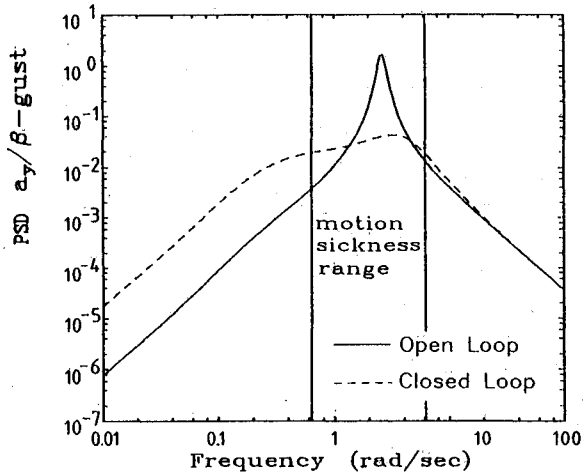

Fig. 9 Acceleration power spectrum due to gust with and without RQAS operating.

Table 2 Open- and closed-loop eigenvalues

	Z domain		*S* domain			
	Real	Imaginary	Real	Imaginary	Frequency, rad/s	Damping
Open-loop longitudinal			−0.0086	0.1028	0.1032 (phugoid)	0.0829
			−0.0086	−0.1028		
			−4.2157	1.5299	4.4848 (short period)	0.9400
			−4.2157	−1.5299		
Closed-loop longitudinal	0.9989	0.0008	−0.0565	0.0400	0.0692	0.8163
	0.9989	−0.0008	−0.0565	−0.0400		
	0.9483	0.0000	−2.6541	0.0000		
	0.8631	0.1177	−6.9000	6.7791	9.6730	0.7133
	0.8631	−0.1177	−6.9000	−6.7791		
	0.7952	0.0000	−11.4558	0.0000		
Open-loop lateral			0.0030	0.0000	(spiral)	
			−2.3855	0.0000	(roll)	
			−0.2222	2.5990	2.6085 (Dutch roll)	0.0852
			−0.2222	−2.5990		
Closed-loop lateral	0.9652	0.0061	−1.7703	0.3172	1.7985	0.9843
	0.9652	−0.0061	−1.7703	−0.3172		
	0.9486	0.0594	−0.25390	3.1279	4.0287	0.6302
	0.9486	−0.0594	−2.5390	−3.1279		
	0.9046	0.0000	−5.0114	0.0000		
	0.8394	0.0000	−8.7563	0.0000		

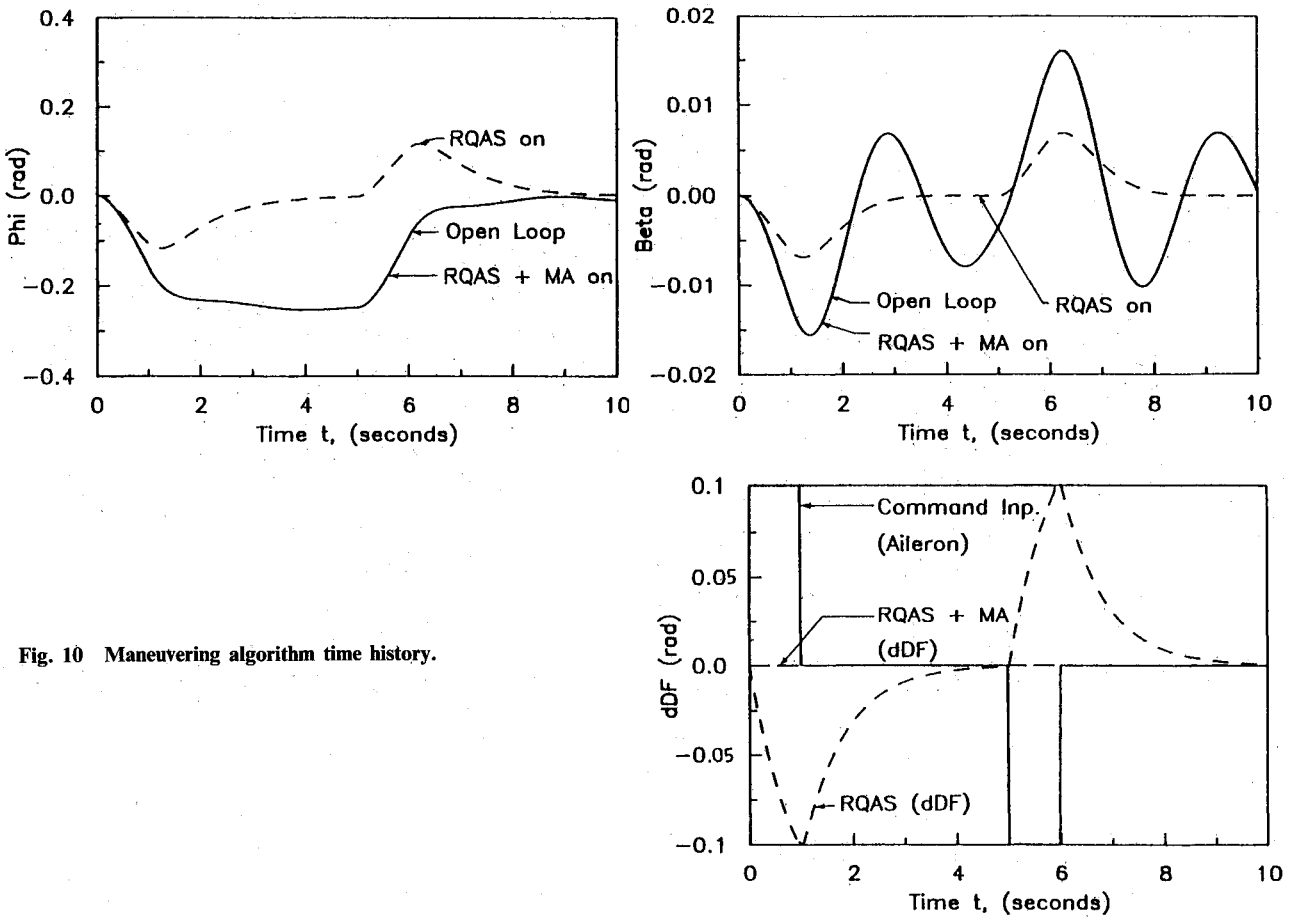

Fig. 10 Maneuvering algorithm time history.

low frequencies. The rms value of the acceleration is given by the square root of the integral of the PSD curve. Since the main contribution to the rms value is the Dutch roll peak, which is well damped in the closed-loop case, as seen in Fig. 7, the rms value is reduced significantly.

Looking at the motion sickness range,[20] which is marked in the figures, one can see that the RQAS drastically reduces the vertical and lateral accelerations in this range. Again, the longitudinal accelerations are amplified, but their magnitude remains small. This shows that the RQAS will greatly increase passenger comfort.

The seemingly poor performance of the controller in cancelling low-frequency lateral accelerations stems from the selection of the weighting matrix elements. The current design puts the main weights on sideslip and yaw rates rather than on the lateral acceleration so that the lateral controller acts mainly as yaw damper.

The damping of the oscillatory modes, i.e., the phugoid and the Dutch roll, also can be observed by looking at the eigenvalues of the closed-loop system given in Table 2. The damping on the phugoid, for example, increases to 0.8. Note that the closed-loop system has two extra poles because of servo dynamics.

Maneuvering Simulation

To demonstrate the effect of the maneuvering algorithm, which is one form of explicit model-following, one sample case is presented here. The pilot input is a 1-s step input to the ailerons, a pause of 4 s, and a 1-s step in the opposite direction. The airplane should bank into a turn and, after 4 s, return to straight and level flight.

Figure 10 shows the bank angle, sideslip, and differential flap deflection as calculated by a linear simulation for three cases: open loop, RQAS on, and RQAS + maneuvering algorithm (MA) on. It is clearly seen that the RQAS fights the pilot input. The moment the airplane starts to roll, it moves the differential flaps to counteract that motion. The maneuvering algorithm, on the other hand, completely ignores the motion, since the command model goes through the same maneuver. The curves for open loop and RQAS + MA are identical, and the RQAS control surfaces do not move at all. The algorithm cannot, however, be expected to work this accurately in the real airplane. It is only exact when the command model exactly matches the airplane dynamics. This is true in the linear simulation presented here.

The sideslip shows the excitation of the Dutch roll mode in this maneuver. As the RQAS has a high damping on all oscillatory modes, it is much reduced with the RQAS on. The use of the command model, however, reintroduces this poorly damped mode. The use of different command models to damp this oscillation is currently being investigated. The RQAS requires all the rudder; therefore, the pilot must fly the airplane without it, except in an emergency. Proper selection of the command model could also ensure coordinated turns without the pilot using the rudder.

Conclusions

A detailed analysis of one set of control algorithms proposed for a commuter aircraft ride-quality augmentation system has been presented. The algorithms include a control law designed using output weighting, an angle of attack and sideslip estimator, and a maneuvering algorithm. The equations for the algorithms have been shown, and derivations can be found in the references. The reductions in vertical accelerations are about 40%, while the longitudinal acceleration increases. However, the longitudinal acceleration rms value remains below 1 ft/s^2 in all cases. The most significant reduction in gust-induced acceleration occurs in the frequency

range of 0.6–6 rad/s, which is the frequency range associated with motion sickness.

The maneuvering algorithm causes the augmented airplane to follow the open-loop airplane exactly in linear time simulations. It is recognized that the command model is only an approximation of the real airplane; therefore, the augmented airplane will follow the command model and not necessarily the actual open-loop airplane. The proper selection of the command model should allow the algorithm to damp the Dutch roll mode and coordinate turns while still following the pilot's commands.

Acknowledgments

This work was supported by the NASA Langley Research Center under Grant NAG1-345. The grant monitor is Earl Hastings. This support is gratefully appreciated.

References

[1]"Airline President Predicts Demise of Independent U.S. Commuters," *Aviation Week & Space Technology*, Vol. 127, June 29, 1987, p. 53.

[2]Richards, L. G., Kuhlthau, A. R., and Jacobson, I. D., *Passenger Ride Quality Determined from Commercial Airline Flights,* NASA TM X-3295, Nov. 1975, pp. 409–436.

[3]Moynes, J. F. and Gallagher, J. T., *Flight Control System Designed for Ride Quality of Highly Maneuverable Aircraft,* Northrop Corp., Hawthorne, CA, N78-26054, 1978.

[4]Roberts, P. A., Swaim, R. L., Schmidt, D. K., and Hinsdale, A. J., *Effect of Control Laws and Relaxed Static Stability on Vertical Ride Quality of Flexible Aircraft*, NASA CR-143843, April 1977.

[5]Holloway, R. D., Thompson, G. O., and Rohling, W. J., "Prospect for Low Wing-Loading STOL Transports with Ride Smoothing," *Journal of Aircraft*, Vol. 9, Aug. 1972, pp. 525–530.

[6]Wykes, J. H. and Borland, C. J., "B-1 Ride Control," *AGARD Active Controls in Aircraft Design*, N79–16876, Nov. 1978.

[7]Phillips, W. H. and Kraft, C. C., Jr., *Theoretical Study of Some Methods for Increasing the Smoothness of Flight through the Air*, NACA TN-2416, 1951.

[8]Conner, D. W. and Thompson, G. O., *Potential Benefits to Short-Haul Transports through the Use of Active Controls*, AGARD CP-157, Paper 3, Oct. 1974.

[9]Krag, B., *Active Control Technology for Gust Alleviation*, Von-Karman Institute Lecture Series 1979-1, Rhode-Saint-Genese, Belgium, Jan. 1979.

[10]Lapins, M. and Jacobson, I. D., *Applications of Active Control Technology to Aircraft Ride Smoothing Systems*, NASA CR-145980, May 1975.

[11]Downing, D. R., Hammond, T. A., and Amin, S. P., *Ride Quality Systems for Commuter Aircraft*, NASA CR-166118, May 1983.

[12]Hammond, T. A., Amin, S. P., Paduano, J. D., and Downing, D. R., *Design of a Digital Ride Quality Augmentation System for Commuter Aircraft*, NASA CR-172419, Oct. 1984.

[13]Davis, D. J., *Preliminary Control Law and Hardware Designs for a Ride Quality Augmentation System for Commuter Aircraft*, NASA CR-4014, Sept. 1986.

[14]Davis, D. J., Jr., *A Comparison of Two Optimal Regulator Design Techniques for the Weighting of Output Variables which are Linear Combinations of States and Controls*, M.S. Thesis, Univ. of Kansas, Lawrence, KS. 1986.

[15]Dorato, P. and Louis, A. H., "Optimal Linear Regulators: The Discrete-Time Case," *IEEE Transactions on Automatic Control*, Vol. AC-16, Dec. 1971.

[16]*Ctrl-C*, Systems Control Technology, Inc., Version 4.0, Sept. 1986.

[17]*Interactive Control Augmentation Design*, Univ. of Kansas Center for Research, Inc., Lawrence, KS, 1985.

[18]Roskam, J., *Airplane Flight Dynamics and Automatic Flight Controls, Part I*, Roskam Aviation and Engineering Corp., Ottawa, KS, 1979.

[19]Heath, R. E., *State Variable Model of Windgusts*, AFFDL/FGC-TM-72, 1982.

[20]Boehret, H. and Krag, B., *OLGA, an Open Loop Gust Alleviation System*, AGARD CP-384.

[21]"Military Specification: Flying Qualities of Piloted Airplanes," MIL-F-8785C (ASG), Aug. 1969.